

Article

Thermal Buckling and Vibration Analysis of SMA Hybrid Composite Sandwich Beams

Mohammad Nejati ^{1,2} , Seyed Sajad Jafari ³, Rossana Dimitri ⁴  and Francesco Tornabene ^{4,*} ¹ Faculty of Mechanical Engineering, Semnan University, Semnan 35131-19111, Iran² Department of Mechanical Engineering, Razi University, Kermanshah 67149-67346, Iran³ Young Researchers & Elite Club, Hamedan Branch, Islamic Azad University, Hamedan 14778-93855, Iran⁴ Department of Innovation Engineering, University of Salento, 73100 Lecce, Italy

* Correspondence: francesco.tornabene@unisalento.it

Abstract: This work studies the buckling and free vibration behavior of Shape Memory Alloy Hybrid Composite (SMAHC) sandwich beams under a thermal environment. The sandwich beams consist of layers reinforced with SMAs and a FGM core, and they are simply supported at both ends. The higher order theory is combined with the Minimum Potential Energy principle or Hamilton principle to derive the governing equations of the thermal buckling and thermal vibration problems, respectively. The material properties of the beam are assumed as temperature-independent (TID) or temperature-dependent (TD). In the last case, two different types of thermal distribution are considered, namely a uniform and a linear distribution. The results based on the proposed formulation are verified against the reference literature, with a very good matching. A parametric study checks for the influence of different effective parameters such as thickness-to-length ratios, volume fraction powers, initial strain, volume fraction of SMA wires, and temperature distribution on the overall mechanical response of the selected structural member, with useful insights from a design standpoint.

Keywords: high order theory; SMAHC sandwich beam; thermal buckling; thermal vibration; uniform and linear temperature distribution



Citation: Nejati, M.; Jafari, S.S.; Dimitri, R.; Tornabene, F. Thermal Buckling and Vibration Analysis of SMA Hybrid Composite Sandwich Beams. *Appl. Sci.* **2022**, *12*, 9323. <https://doi.org/10.3390/app12189323>

Academic Editor: Diogo Ribeiro

Received: 8 August 2022

Accepted: 14 September 2022

Published: 17 September 2022

Publisher's Note: MDPI stays neutral with regard to jurisdictional claims in published maps and institutional affiliations.



Copyright: © 2022 by the authors. Licensee MDPI, Basel, Switzerland. This article is an open access article distributed under the terms and conditions of the Creative Commons Attribution (CC BY) license (<https://creativecommons.org/licenses/by/4.0/>).

1. Introduction

Today, sandwich structures are largely applied in many industrial applications, primarily in aerospace, marine, transportation, and civil applications due to their special properties, including lightweight, high stiffness, strength, and damping capability. Sandwich structures typically consist of two external layers and an internal core. The layer materials are usually made of metals [1], composites [2], or fiber-metal-laminate [3], whereas the core material includes foam [4], honeycomb [5], or Functionally-Graded materials (FGMs) [6]. The introduction of Shape Memory Alloys (SMAs) within the top/bottom layers is an efficient way to improve the sandwich properties. Intelligent materials such as SMAs, have some unique properties, such as a large recoverable strain field, together with a high flexibility shape memory effect and pseudo-elasticity [7]. On the other hand, a large recovery strain field and a certain flexibility of the SMAs for different load histories, temperatures, and stresses can be obtained for tunable thermal and mechanical properties [8].

In recent decades, different works from literature have shown an increased interest in the buckling and post-buckling behavior of composite plates, shells, and beams embedding SMAs [9–13]. Girish and Ramachandra [14] used a higher order shear deformation theory (HSDT) to study the buckling response of composite plates subjected to a uniform temperature distribution throughout the thickness. Kamarian and Shakeri [15] focused on an optimized buckling response of rectangular and skew composite plates in thermal environments by embedding different quantities of SMA wires. The authors applied the First Order Shear Deformation Theory (FSDT) and used a Generalized Differential Quadrature (GDQ) method to solve the governing equations of the problem. The Von Karman nonlinear

displacement–strain relationships were used by Ho Roh et al. [16] to investigate the thermal post buckling of shape memory alloy hybrid composite shell panels. In such work, it was shown that the snapping phenomenon of shells can be prevented by embedding SMA wires in a composite structure.

Buckling and post-buckling phenomena are particularly important for structural beams in thermal conditions [17,18]. One well-known method to increase the thermal buckling resistance of sandwich beams relies on the introduction of SMAs into these structures [19]. Khdeir [20] studied the variation of the critical buckling temperature of cross-ply beams with various boundary conditions. The author also reported the effect of some parameters such as the length-to-thickness ratio and thermal expansion coefficients ratio on the critical buckling temperature. Bayat and Ekhteraei Toussi [21] applied a Layer-Wise Theory (LWT) to explore the thermal buckling and post-buckling behavior of laminated composite beams reinforced with SMA wires. The authors studied the effect of some parameters on the mechanical response, including the symmetric and antisymmetric layups, as well as the influence of the thickness/span ratio, SMA pre-strain, and volume fraction.

The free vibration of composite structures is another important aspect to investigate, as extensively found in literature [8,22,23]. Sang Park et al. [24] performed a vibration analysis of the composite plates embedded with shape memory alloy fibers by combining the FSDT basics with the Von Karman strain–displacement relations. Based on their results, the plates increased their stiffness for an increased volume fraction and initial strain of the SMA fibers; the authors also checked for the optimal design of fiber angle, stacking sequence, volume fraction, and initial strain of the SMAs.

Similarly, Parhi and Singh [25] studied the free vibration of SMA-embedded laminated composite shell panels, including spherical and cylindrical shell panels with TD material properties. The authors used a HSDT combined with the principle of virtual work and non-linear von Karman strain displacement relations to handle the problem. Nekouei et al. [26] analyzed the free vibration of hybrid laminated composite cylindrical shells reinforced with SMA by applying the Brinson's one-dimensional constitutive law to calculate the thermo-mechanical properties of SMAs. According to the study, the fundamental frequency was increased by adding a proper quantity of SMA wires to the cylindrical shells. At the same time, Roger and Barker [27] showed that the SMA wire heating induces an axial stress in the graphite–epoxy composite beam, where the introduction of 15% volume fraction of SMA wires is capable of increasing the overall natural frequency. Asadi et al. [28] studied the free vibration of thermally pre/post-buckled shear deformable SMA hybrid composite beams. The problem was tackled theoretically based on the FSDT, von Karman geometrical non-linearity, and extended Hamilton principle. The authors, in their work, verified a general improvement of the buckling temperature and post-buckling path of the shape memory alloy hybrid composite (SMAHC) beam by concentrating the SMA fibers in the center of the laminated beam. In addition, Alambeigi et al. [29] analyzed the free and forced vibration of sandwich beams made of a functionally-graded porous core and composite face layers embedding SMAs, immersed within an elastic foundation, modeled according to the Vlasov basics. Once again, it was found that the temperature, volume fraction of SMA, and porosity distribution are important parameters affecting the overall response of sandwich beams. Starting with the available literature on the topic, the present work is aimed at investigating the vibration and buckling response of sandwich beams with SMA reinforced external layers and a FGM core, under thermal conditions. More specifically, two types of thermal distribution are considered, namely, a linear and a uniform distribution. The governing equations for the thermal buckling and vibration rely on a high order theory, combined with the Minimum Potential Energy principle or Hamilton principle, respectively. To verify the accuracy of the proposed analytical method, our results are successfully compared to well-known references from literature. A large sensitivity analysis is, thus, performed to check for the effect of some important parameters such as types of thermal

load, volume fraction, and initial pre-strained SMA wires, as well as different geometrical properties for both the face sheets and the core of the selected sandwich structure.

2. Materials Properties and Basic Equations of SMA

Let us consider a composite beam made of two layers and an FGM core. In more detail, the external layers are made of a graphite–epoxy composite with the addition of a SMA reinforcement. The selected structural member is here studied based on the Brinson’s model [30], due to its capability in considering the thermo-mechanical behavior at any temperature. According to this model, we introduce the following relation between the stress field, σ , strain field, ε , thermal field, T , martensite fraction, ξ , Young’s modulus of the SMA, $E(\varepsilon, \xi, T)$, transformation tensor, $\Omega(\xi)$, and thermal tensor, Θ , i.e.,

$$d\sigma = E(\varepsilon, \xi, T) d\varepsilon + \Omega(\varepsilon, \xi, T)d\xi_s + \Theta(\varepsilon, \xi, T) dT \tag{1}$$

The Young’s modulus of the SMA is expressed as [31]:

$$E(\varepsilon, \xi, T) = E(\xi) = \frac{E_A}{1 + \xi \left(\frac{E_A}{E_M} - 1 \right)} \tag{2}$$

where E_A and E_M are the Young’s moduli of a perfect austenite and martensite state, respectively. The martensite fraction is the summation of two parameters, i.e., the stress rise, ξ_s , and temperature rise, ξ_T . In addition, the transformation tensor is defined as:

$$\Omega(\xi) = -\varepsilon_L E(\xi) \tag{3}$$

where ε_L is the maximum residual strain of the SMA wires obtained during a uniaxial tension test. There are two phases to measure the martensite fractions, depending on temperature and stress: (I) the phase transformation to M (martensite), (II) the phase transformation from M (martensite) to A (austenite). Phase (I) is described by the following equations:

If $T > M_s$ and $\sigma_s^{cr} + C_M(T - M_s) < \sigma < \sigma_f^{cr} + C_M(T - M_f)$

$$\begin{aligned} \xi_s &= \frac{1 - \xi_{s0}}{2} \cos\left(\frac{\pi}{\sigma_s^{cr} - \sigma_f^{cr}}(\sigma - \sigma_f^{cr} - C_M(T - M_s))\right) + \frac{1 + \xi_{s0}}{2} \\ \xi_T &= \xi_{T0} - \frac{\xi_{T0}}{1 - \xi_{s0}}(\xi_s - \xi_{s0}) \end{aligned} \tag{4}$$

If $T < M_s$ and $\sigma_s^{cr} < \sigma < \sigma_f^{cr}$

$$\begin{aligned} \xi_s &= \frac{1 - \xi_{s0}}{2} \cos\left(\frac{\pi}{\sigma_s^{cr} - \sigma_f^{cr}}(\sigma - \sigma_f^{cr})\right) + \frac{1 + \xi_{s0}}{2} \\ \xi_T &= \xi_{T0} - \frac{\xi_{T0}}{1 - \xi_{s0}}(\xi_s - \xi_{s0}) + \Delta T \xi \end{aligned} \tag{5}$$

If $M_f < T < M_s$ and $T < T_0$

$$\Delta T \xi = \frac{1 - \xi_{T0}}{2} \left(\cos(a_M(T - M_f)) + 1 \right) \tag{6}$$

Otherwise, $\Delta T \xi = 0$. Phase (II), instead, accounts for the following relations:

If $T > A_s$ and $C_A(T - A_f) < \sigma < C_A(T - A_s)$

$$\begin{aligned} \xi &= \frac{\xi_0}{2} \left(\cos \left[\frac{\pi}{A_f - A_s} (T - A_s - \frac{\sigma}{C_A}) \right] + 1 \right) \\ \xi_s &= \xi_{s0} - \frac{\xi_{s0}}{\xi_0} (\xi_0 - \xi) \\ \xi_T &= \xi_{T0} - \frac{\xi_{T0}}{\xi_0} (\xi_0 - \xi) \\ C_A &= \left(\frac{dA_s}{d\sigma} \right)^{-1}, C_M = \left(\frac{dM_s}{d\sigma} \right)^{-1} \end{aligned} \tag{7}$$

where the subscript 0 refers to the initial state and M_f , M_s , A_s , and A_f are the martensite finish temperature, martensite start temperature, austenite start temperature, and austenite finish temperature, respectively. C_A and C_M refer to the transformation constants for the austenite and martensite phases, respectively. More details regarding the mechanical properties of SMAs can be found in Table 1, accordingly to [30]. The relations defining the properties of a graphite–epoxy reinforced with SMAs (NiTi wires) with TD conditions are mentioned in Appendix A, whose properties are reported in Table 2, in line with [31].

Table 1. Material properties of SMA wires.

$E_A = 67$ GPa	$C_M = 8$ MPa/°C
$E_M = 26.3$ GPa	$C_A = 13.8$ MPa/°C
$M_f = 9$ °C	$v_s = 0.33$
$M_s = 18.4$ °C	$\alpha_s = 10.26$ °C
$A_f = 34.5$ °C	$\theta = 0.55$ MPa/°C
$A_s = 49$ °C	$\sigma_s^{cr} = 100$ MPa
$\epsilon_L = 0.067$	$\sigma_f^{cr} = 170$ MPa

Table 2. Thermomechanical properties of the layers.

$E_{1m} = E_{1m}^0 (1 + E_{1m}^1 \Delta T)$	$E_{1m}^0 = 155$ GPa	$E_{1m}^1 = -3.53 \times 10^{-4}$
$E_{2m} = E_{2m}^0 (1 + E_{2m}^1 \Delta T)$	$E_{2m}^0 = 8.07$ GPa	$E_{2m}^1 = -4.27 \times 10^{-4}$
$G_{12m} = G_{12m}^0 (1 + G_{12m}^1 \Delta T)$	$G_{12m}^0 = 4.55$ GPa	$G_{12m}^1 = -6.06 \times 10^{-4}$
$G_{23m} = G_{23m}^0 (1 + G_{23m}^1 \Delta T)$	$G_{23m}^0 = 3.25$ GPa	$G_{23m}^1 = -6.06 \times 10^{-4}$
$\alpha_{1m} = \alpha_{1m}^0 (1 + \alpha_{1m}^1 \Delta T)$	$\alpha_{1m}^0 = -0.07 \times 10^{-6}$	$\alpha_{1m}^1 = -1.25 \times 10^{-3}$
$\alpha_{2m} = \alpha_{2m}^0 (1 + \alpha_{2m}^1 \Delta T)$	$\alpha_{2m}^0 = 30.1 \times 10^{-6}$	$\alpha_{2m}^1 = 0.41 \times 10^{-4}$
$v_{12m} = 0.22$		
$\rho_m = 1586$ kg/m ³		

To define the variation of an arbitrary property throughout the thickness, such as the Young’s modulus (E), the coefficient of thermal expansion (α), or the density (ρ), we introduce the following relation:

$$P(z) = (P_c - P_m)(z/h_c + 1/2)^n + P_m \tag{8}$$

where the subscripts c and m refer to a ceramic and metal phase, respectively, and h_c and n stand for the FGM thickness and volume fraction power, respectively. Similarly to face sheets, the mechanical properties of the FGM core are TD.

As FGMs are most commonly used in high temperature conditions with significant variations of material properties, it is reliable to assume TD mechanical properties for FGM cores to ensure an accurate prediction of the structural response. The material properties

of the ceramic and metal phases are expressed as non-linear functions of the environment temperature; see [32,33]

$$P_i(T) = P_0(P_{-1} + 1 + P_1 T + P_2 T^2 + P_3 T^3) \quad i = c, m \tag{9}$$

where T is the temperature in Kelvin and P_i ($i = -1, 0, 1, 2, 3$) refers to the TD constants, as defined in Table 3 [33].

Table 3. TD constants of metal and ceramic phases.

Properties	Materials	P_0	P_{-1}	P_1	P_2	P_3
Young's elasticity modulus	Ti-6Al-4V	122.56×10^9	0	-4.586×10^{-4}	0	0
	Zirconia	244.27×10^9	0	-1.371×10^{-3}	1.214×10^{-6}	-3.681×10^{-10}
Coefficient of Thermal Expansion	Ti-6Al-4V	7.5788×10^{-6}	0	6.638×10^{-4}	-3.147×10^{-6}	0
	Zirconia	12.766×10^{-6}	0	-1.491×10^{-3}	1.006×10^{-5}	-6.778×10^{-11}
density	Ti-6Al-4V	4429	0	0	0	0
	Zirconia	5700	0	0	0	0

3. Governing Equations Derivation

In this section, we describe the theoretical formulation here adopted to study the thermal buckling and vibration of a sandwich beam with an FGM core of thickness h_c and SMA hybrid layers of thickness h_a , as depicted in Figure 1.

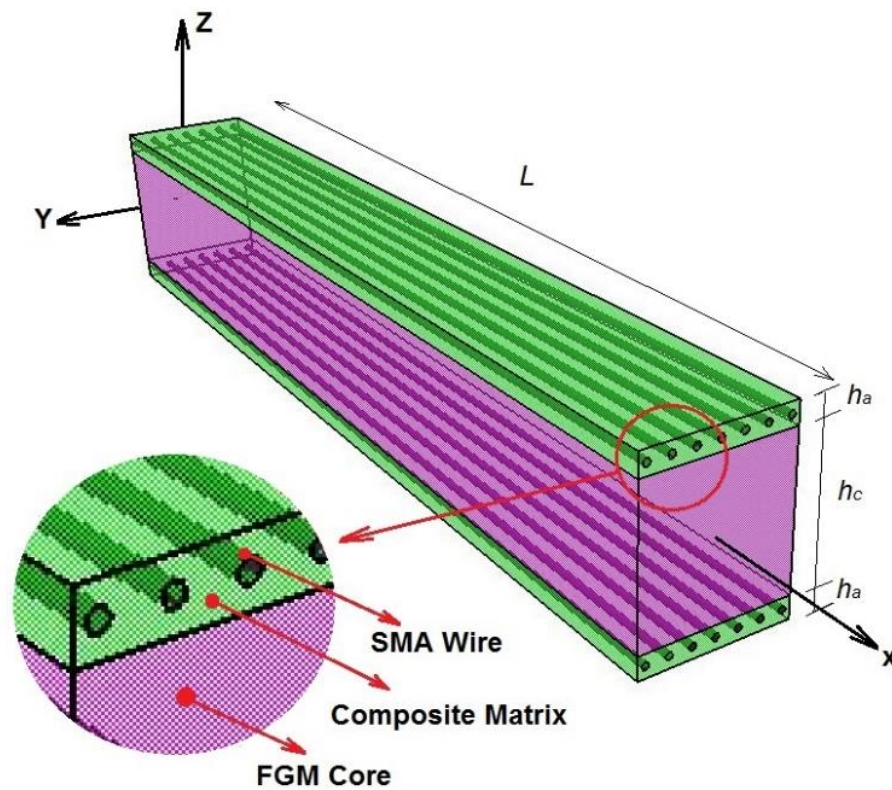


Figure 1. Sandwich beam with an FGM core and SMA reinforcement layers.

3.1. Equilibrium Equations

The analysis of the SMAHC sandwich beam is based on a HSDT, such that the displacement field, $\bar{u}(x, z, t)$, $\bar{v}(x, z, t)$, $\bar{w}(x, z, t)$, is defined as [34]:

$$\begin{aligned} \bar{u}(x, z, t) &= u_0(x, t) + \frac{5}{4} \left(z - \frac{4}{3h^2} z^3 \right) \phi_x(x, t) + \left(\frac{1}{4} z - \frac{5}{3h^2} z^3 \right) \frac{\partial w_0(x, t)}{\partial x} \\ \bar{v}(x, z, t) &= 0 \\ \bar{w}(x, z, t) &= w_0(x, t) \end{aligned} \tag{10}$$

where u_0 and w_0 are the displacement components along the x and z coordinate directions, respectively, of a point on the mid-surface. In addition, ϕ_x refers to the rotation about the x axis and h is the total beam thickness. The kinematic relations at Cartesian coordinates (x - y - z) are defined as [34]:

$$\begin{aligned} \varepsilon_x &= \frac{\partial \bar{u}}{\partial x} + \frac{1}{2} \left(\frac{\partial \bar{w}}{\partial x} \right)^2, \quad \varepsilon_y = \frac{\partial \bar{v}}{\partial y}, \quad \varepsilon_z = \frac{\partial \bar{w}}{\partial z}, \quad \gamma_{xy} = \frac{\partial \bar{u}}{\partial y} + \frac{\partial \bar{v}}{\partial x}, \\ \gamma_{xz} &= \frac{\partial \bar{u}}{\partial z} + \frac{\partial \bar{w}}{\partial x} + \frac{\partial \bar{w}}{\partial x} \frac{\partial \bar{w}}{\partial z}, \quad \gamma_{yz} = \frac{\partial \bar{v}}{\partial z} + \frac{\partial \bar{w}}{\partial y} \end{aligned} \tag{11}$$

By substituting Equation (10) into Equation (11), we obtain the following equation:

$$\begin{aligned} \varepsilon_x &= \varepsilon_x^{(0)} + z\varepsilon_x^{(1)} + z^3\varepsilon_x^{(3)} \\ \gamma_{xz} &= \gamma_{xz}^{(0)} + z^2\gamma_{xz}^{(2)} \end{aligned} \tag{12}$$

where $\varepsilon_x^{(0)}$, $\varepsilon_x^{(1)}$, $\varepsilon_x^{(3)}$, $\gamma_{xz}^{(0)}$, and $\gamma_{xz}^{(2)}$ are defined as:

$$\begin{pmatrix} \varepsilon_x^{(0)} \\ \varepsilon_x^{(1)} \\ \varepsilon_x^{(3)} \end{pmatrix} = \begin{pmatrix} \frac{du}{dx} + \frac{1}{2} \left(\frac{dw_0}{dx} \right)^2 \\ \frac{5}{4} \frac{d\phi_x}{dx} + \frac{1}{4} \frac{d^2w_0}{dx^2} \\ - \left(\frac{5}{3h^2} \frac{d\phi_x}{dx} + \frac{5}{3h^2} \frac{d^2w_0}{dx^2} \right) \end{pmatrix}, \quad \begin{pmatrix} \gamma_{xz}^{(0)} \\ \gamma_{xz}^{(2)} \end{pmatrix} = \begin{pmatrix} \frac{5}{4} \phi_x + \frac{5}{4} \frac{dw_0}{dx} \\ - \left(\frac{5}{h^2} \phi_x + \frac{5}{h^2} \frac{dw_0}{dx} \right) \end{pmatrix} \tag{13}$$

The equilibrium equations are obtained according to the HSDT and the Principal of Minimum Potential Energy (PMPE), expressed as [34]:

$$\Pi = U - W \tag{14}$$

where U and W refer to the strain energy and the external work, respectively, defined in variational form δ [35] as follows:

$$\delta U = \int_{\Omega} (\sigma_x \delta \varepsilon_x + \sigma_{xz} \delta \gamma_{xz}) dx dz \tag{15}$$

or equivalently:

$$\begin{aligned} \delta U &= \int_0^L \int_{-(\frac{h_c}{2} + h_a)}^{\frac{h_c}{2} + h_a} \sigma_x \left\{ \begin{aligned} &\frac{d\delta u}{dx} + \frac{dw_0}{dx} \frac{d\delta w_0}{dx} + \left(\frac{5}{4} \frac{d\delta \phi_x}{dx} + \frac{1}{4} \frac{d^2\delta w_0}{dx^2} \right) z - \\ &\left(\frac{5}{3h^2} \frac{d\delta \phi_x}{dx} + \frac{5}{3h^2} \frac{d^2\delta w_0}{dx^2} \right) z^3 \end{aligned} \right\} dz + \\ &\sigma_{xz} \left(\frac{5}{4} \delta \phi_x + \frac{5}{4} \frac{d\delta w_0}{dx} - \left(\frac{5}{h^2} \delta \phi_x + \frac{5}{h^2} \frac{d\delta w_0}{dx} \right) z^2 \right) dz dx \end{aligned} \tag{16}$$

At the same time, Equation (16) can be redefined in terms of resultants ($N_x, M_x, N_{xz}, P_x, R_{xz}$), i.e.,

$$\begin{aligned} \delta U = & \int_0^L \left(N_x \left(\frac{d\delta u}{dx} + \frac{dw_0}{dx} \frac{d\delta w_0}{dx} \right) + M_x \left(\frac{5}{4} \frac{d\delta \phi_x}{dx} + \frac{1}{4} \frac{d^2\delta w_0}{dx^2} \right) + \right. \\ & P_x \left(\frac{5}{3h^2} \frac{d\delta \phi_x}{dx} + \frac{5}{3h^2} \frac{d^2\delta w_0}{dx^2} \right) + N_{xz} \left(\frac{5}{4} \delta \phi_x + \frac{5}{4} \frac{d\delta w_0}{dx} \right) + \\ & \left. R_{xz} \left(- \left(\frac{5}{h^2} \delta \phi_x + \frac{5}{h^2} \frac{d\delta w_0}{dx} \right) \right) \right) dx \end{aligned} \tag{17}$$

where N_x is the in-plane force resultants; M_x is the moment resultants; N_{xz} is the final transverse force resultants; and P_x and R_{xz} are the stressed higher order resultants determined as a sum of the mechanical, thermal, and recovery resultants (denoted with superscript M, T, and r, respectively). Such parameters are defined as:

$$\begin{aligned} N_x = & N_x^M + N_x^T + N_x^r = \int_{-(h_c/2+h_a)}^{h_c/2+h_a} (\sigma_x^M + \sigma_x^T) dz + \int_{-(h_c/2+h_a)}^{-h_c/2} \sigma_x^r dz + \int_{h_c/2}^{h_c/2+h_a} \sigma_x^r dz \\ M_x = & M_x^M + M_x^T + M_x^r = \int_{-(h_c/2+h_a)}^{h_c/2+h_a} z(\sigma_x^M + \sigma_x^T) dz + \int_{-(h_c/2+h_a)}^{-h_c/2} z\sigma_x^r dz + \int_{h_c/2}^{h_c/2+h_a} z\sigma_x^r dz \\ N_{xz} = & N_{xz}^M + N_{xz}^T + N_{xz}^r = \int_{-(h_c/2+h_a)}^{h_c/2+h_a} (\sigma_{xz}^M + \sigma_{xz}^T) dz + \int_{-(h_c/2+h_a)}^{-h_c/2} \sigma_{xz}^r dz + \int_{h_c/2}^{h_c/2+h_a} \sigma_{xz}^r dz \\ P_x = & P_x^M + P_x^T + P_x^r = \int_{-(h_c/2+h_a)}^{h_c/2+h_a} z^3(\sigma_x^M + \sigma_x^T) dz + \int_{-(h_c/2+h_a)}^{-h_c/2} z^3\sigma_x^r dz + \int_{h_c/2}^{h_c/2+h_a} z^3\sigma_x^r dz \\ R_{xz} = & R_{xz}^M + R_{xz}^T + R_{xz}^r = \int_{-(h_c/2+h_a)}^{h_c/2+h_a} z^2(\sigma_{xz}^M + \sigma_{xz}^T) dz + \int_{-(h_c/2+h_a)}^{-h_c/2} z^2\sigma_{xz}^r dz + \int_{h_c/2}^{h_c/2+h_a} z^2\sigma_{xz}^r dz \end{aligned} \tag{18}$$

Finally, from Equation (17), the equilibrium equations can be obtained as:

$$\begin{aligned} \delta u_0 = 0 \Rightarrow & \frac{dN_x}{dx} = 0 \\ \delta \phi_x = 0 \Rightarrow & -\frac{5}{4} \frac{dM_x}{dx} + \frac{5}{3h^2} \frac{dP_x}{dx} + \frac{5}{4} N_{xz} - \frac{5}{h^2} R_{xz} = 0 \\ \delta w_0 = 0 \Rightarrow & -\frac{d}{dx} \left(N_x \frac{dw_0}{dx} \right) + \frac{1}{4} \frac{d^2M_x}{dx^2} - \frac{5}{3h^2} \frac{d^2P_x}{dx^2} - \frac{5}{4} \frac{dN_{xz}}{dx} + \frac{5}{h^2} \frac{dR_{xz}}{dx} = 0 \end{aligned} \tag{19}$$

In addition, the stress-strain ($\sigma - \varepsilon$) relation involving the recovery stress and thermal strain at Cartesian coordinates are defined as:

$$\begin{pmatrix} \sigma_x \\ \sigma_y \\ \sigma_z \\ \sigma_{yz} \\ \sigma_{xz} \\ \sigma_{xy} \end{pmatrix} = \begin{bmatrix} C_{11} & C_{12} & C_{13} & 0 & 0 & 0 \\ C_{12} & C_{22} & C_{23} & 0 & 0 & 0 \\ C_{13} & C_{23} & C_{33} & 0 & 0 & 0 \\ 0 & 0 & 0 & C_{44} & 0 & 0 \\ 0 & 0 & 0 & 0 & C_{55} & 0 \\ 0 & 0 & 0 & 0 & 0 & C_{66} \end{bmatrix} \left(\begin{pmatrix} \varepsilon_x \\ \varepsilon_y \\ \varepsilon_z \\ \gamma_{yz} \\ \gamma_{xz} \\ \gamma_{xy} \end{pmatrix} - \begin{pmatrix} \alpha_x \\ \alpha_y \\ \alpha_z \\ 0 \\ 0 \\ 0 \end{pmatrix} \Delta T \right) + V_s \begin{pmatrix} \sigma_1^r \\ \sigma_2^r \\ 0 \\ 0 \\ 0 \\ \sigma_{12}^r \end{pmatrix} \tag{20}$$

where C_{ij} ($i, j = 1, 2, \dots, 6$) are the stiffness matrix components. In addition, α_i ($i = x, y, z$), ΔT stand for the thermal expansion and thermal variation, and V_s and σ_{ij}^r ($i, j = 1, 2, 3$) refer to the volume fraction and recovery stress of the shape memory alloy, respectively. Thus, the mechanical and thermal stresses are defined as:

$$\begin{Bmatrix} \sigma_x^M \\ \sigma_{xz}^M \end{Bmatrix} = \begin{Bmatrix} C_{11}\varepsilon_x \\ C_{55}\gamma_{xz} \end{Bmatrix}, \quad \begin{Bmatrix} \sigma_x^T \\ \sigma_{xz}^T \end{Bmatrix} = \begin{Bmatrix} C_{11}\alpha_x\Delta T \\ 0 \end{Bmatrix} \tag{21}$$

Moreover, the relations between the stress resultants and the displacement field are obtained by combining Equation (18) and the stress-displacement relation, as briefly described in Appendix A (A5–A7). Finally, the equilibrium Equation (19) has been obtained according to the displacement field, u_0, ϕ_x, w_0 .

3.2. Stability Equations

We now determine the stability equations of the beam under a thermal condition. The expansion of the total potential energy (V) based on the Taylor series reads as follows [36]:

$$\Delta V = \delta V + \frac{1}{2}\delta^2 V + \frac{1}{6}\delta^3 V + \dots \quad (22)$$

where δV is the first variation of the total potential energy, which is related to the equilibrium state, whereas the second variation, $\delta^2 V$, is representative of the stability in the neighborhood of the equilibrium state. For all virtual displacements, if $\delta^2 V > 0$ the beam remains stable, otherwise ($\delta^2 V < 0$) it becomes unstable. The last condition, $\delta^2 V = 0$, is associated with the critical buckling condition [36]. In fact, the critical thermal buckling load disrupts the stability in equilibrium state. The main reason for obtaining the stability equations is related to the nonlinearity of the equilibrium equations. Let us assume that the displacement components (u_0, ϕ_x, w_0) undergo a small increment:

$$\begin{aligned} u_0 &\rightarrow u_0^0 + u_0^1 \\ \phi_x &\rightarrow \phi_x^0 + \phi_x^1 \\ w_0 &\rightarrow w_0^0 + w_0^1 \end{aligned} \quad (23)$$

where u_0^0, ϕ_x, w_0^0 refer to the displacement field in the equilibrium state, whereas u_0^1, ϕ_x^1, w_0^1 are the associated components of a neighboring stable state in respect of the equilibrium state. The force resultants of a neighboring state are related to the equilibrium state as:

$$\begin{aligned} N_x &\rightarrow N_x^0 + N_x^1 \\ M_x &\rightarrow M_x^0 + M_x^1 \\ P_x &\rightarrow P_x^0 + P_x^1 \\ N_{xz} &\rightarrow N_{xz}^0 + N_{xz}^1 \\ R_{xz} &\rightarrow R_{xz}^0 + R_{xz}^1 \end{aligned} \quad (24)$$

Superscript ‘1’ refers to the stability state and superscript ‘0’ refers to the equilibrium state. By substituting Equations (23) and (24) into the equilibrium equation, Equation (19), a deviation of the force resultants from the initial equilibrium state can be obtained, as detailed in Appendix A, (A8). Finally, the stability equations can be obtained as follows:

$$\begin{aligned} \delta u_0 &= 0 \Rightarrow \frac{dN_x^1}{dx} = 0 \\ \delta \phi_x &= 0 \Rightarrow -\frac{5}{4} \frac{dM_x^1}{dx} + \frac{5}{3h^2} \frac{dP_x^1}{dx} + \frac{5}{4} N_{xz}^1 - \frac{5}{h^2} R_{xz}^1 = 0 \\ \delta w_0 &= 0 \Rightarrow -N_{x0} \frac{d^2 w_0^1}{dx^2} + \frac{1}{4} \frac{d^2 M_x^1}{dx^2} - \frac{5}{3h^2} \frac{d^2 P_x^1}{dx^2} - \frac{5}{4} \frac{dN_{xz}^1}{dx} + \frac{5}{h^2} \frac{dR_{xz}^1}{dx} = 0 \end{aligned} \quad (25)$$

where N_{x0} , for a uniform and linear temperature rise, is defined as:

$$N_{x0} = \int_{-(h_c/2+h_a)}^{(h_c/2+h_a)} C_{ij}(z) \alpha_i(z) (T - T_0) dz, \quad i, j = x, y, z \quad (26)$$

and T_0 is the reference temperature. When the beam buckles at $T = T_0 + \Delta T$, such thermal value will be updated in Equation (26).

Let us now consider a sandwich beam whose temperature at the top and bottom layer surfaces is labeled as T_t and T_b , respectively. The temperature distribution for fixed boundary conditions is obtained by solving the heat conduction equation along the beam thickness. If the beam thickness is thin enough, the temperature distribution is approximated as linear through the thickness direction z .

For a simply supported beam, the displacement components are assumed as:

$$\begin{aligned}
 u_0^1 &= u_m \cos\left(\frac{m\pi x}{L}\right) \\
 \phi_x^1 &= \phi_m \cos\left(\frac{m\pi x}{L}\right) \\
 w_0^1 &= w_m \sin\left(\frac{m\pi x}{L}\right)
 \end{aligned}
 \tag{27}$$

where m is the longitudinal wave number in the x -direction, and u_m, ϕ_m, w_m are the unknown axial functions. Finally, by using Equations (17) and (25) and Appendix A (A8), we obtain the stability equations in terms of u_m, ϕ_m, w_m .

3.3. Free Vibration under Thermal Conditions

We can now determine the equations of motion for the vibration of SMAHC sandwich beams in a thermal environment, based on the Hamilton principle [37]:

$$\int_{t_1}^{t_2} (\delta KE - \delta PE) dt = 0
 \tag{28}$$

where KE is the kinetic energy of the beam and PE is the associated elastic potential energy. More specifically, the kinetic energy of the beam is defined as:

$$KE = \frac{1}{2} \int_0^L \int_{-(h_c/2+h_a)}^{h_c/2+h_a} \rho \left(\left(\frac{\partial \bar{u}}{\partial t}\right)^2 + \left(\frac{\partial \bar{v}}{\partial t}\right)^2 + \left(\frac{\partial \bar{w}}{\partial t}\right)^2 \right) dx dz
 \tag{29}$$

or, after some manipulation:

$$\delta KE = \int_0^L \left(\begin{aligned} & I_0 \left(\frac{\partial u_0}{\partial t} \frac{\partial \delta u_0}{\partial t} + \frac{\partial w_0}{\partial t} \frac{\partial \delta w_0}{\partial t} \right) + I_1 \left(\frac{1}{4} \left(\frac{\partial \delta u_0}{\partial t} \frac{\partial^2 w_0}{\partial x \partial t} + \frac{\partial u_0}{\partial t} \frac{\partial^2 \delta w_0}{\partial x \partial t} \right) + \right. \\ & \left. \frac{5}{4} \left(\frac{\partial \delta u_0}{\partial t} \frac{\partial \phi_x}{\partial t} + \frac{\partial u_0}{\partial t} \frac{\partial \delta \phi_x}{\partial t} \right) \right) + \\ & I_2 \left(\frac{25}{16} \frac{\partial \phi_x}{\partial t} \frac{\partial \delta \phi_x}{\partial t} + \frac{1}{16} \frac{\partial^2 w_0}{\partial x \partial t} \frac{\partial^2 \delta w_0}{\partial x \partial t} + \right. \\ & \left. \frac{5}{16} \left(\frac{\partial \delta \phi_x}{\partial t} \frac{\partial^2 w_0}{\partial x \partial t} + \frac{\partial \phi_x}{\partial t} \frac{\partial^2 \delta w_0}{\partial x \partial t} \right) \right) + \\ & I_3 \left(-\frac{10}{6h^2} \left(\frac{\partial \delta u_0}{\partial t} \frac{\partial \phi_x}{\partial t} + \frac{\partial u_0}{\partial t} \frac{\partial \delta \phi_x}{\partial t} \right) - \right. \\ & \left. \frac{10}{6h^2} \left(\frac{\partial \delta u_0}{\partial t} \frac{\partial^2 w_0}{\partial x \partial t} + \frac{\partial u_0}{\partial t} \frac{\partial^2 \delta w_0}{\partial x \partial t} \right) \right) + \\ & I_4 \left(-\frac{5}{2h^2} \left(\frac{\partial \delta \phi_x}{\partial t} \frac{\partial^2 w_0}{\partial x \partial t} + \frac{\partial \phi_x}{\partial t} \frac{\partial^2 \delta w_0}{\partial x \partial t} \right) - \frac{25}{6h^2} \frac{\partial \phi_x}{\partial t} \frac{\partial \delta \phi_x}{\partial t} - \right. \\ & \left. \frac{5}{6h^2} \frac{\partial^2 w_0}{\partial x \partial t} \frac{\partial^2 \delta w_0}{\partial x \partial t} \right) + \\ & I_6 \left(\frac{50}{18h^4} \left(\frac{\partial \phi_x}{\partial t} \frac{\partial^2 \delta w_0}{\partial x \partial t} + \frac{\partial \delta \phi_x}{\partial t} \frac{\partial^2 w_0}{\partial x \partial t} \right) + \frac{25}{9h^4} \frac{\partial \phi_x}{\partial t} \frac{\partial \delta \phi_x}{\partial t} + \right. \\ & \left. \frac{25}{9h^4} \frac{\partial^2 w_0}{\partial x \partial t} \frac{\partial^2 \delta w_0}{\partial x \partial t} \right) \end{aligned} \right) dx
 \tag{30}$$

where:

$$\begin{aligned}
 (I_0, I_1, I_2, I_3, I_4, I_6) &= \int_{-h_c/2}^{h_c/2} \rho^{FGM}(1, z, z^2, z^3, z^4, z^6) dz + \\ & \int_{h_c/2}^{h_c/2+h_a} \rho^{Top\ layer}(1, z, z^2, z^3, z^4, z^6) dz + \int_{-h_c/2}^{-(h_c/2+h_a)} \rho^{Bottom\ layer}(1, z, z^2, z^3, z^4, z^6) dz
 \end{aligned}
 \tag{31}$$

The elastic potential energy of the beam includes the strain energy due to vibration (PE_p) and the primary stresses due to a thermal increase (PE_T), respectively, namely [37,38]:

$$PE = PE_p + PE_T
 \tag{32}$$

$$PE_p = \int_0^L \int_{-(h_c/2+h_a)}^{h_c/2+h_a} (\sigma_{xx}\epsilon_{xx}^L + \sigma_{xz}\gamma_{xz}^L) dx dz \tag{33}$$

$$PE_T = \int_0^L \int_{-(h_c/2+h_a)}^{h_c/2+h_a} (\sigma_{0xx}\epsilon_{xx}^{NL} + \sigma_{0xz}\gamma_{xz}^{NL}) dx dz \tag{34}$$

where σ_{ij} and σ_{0ij} ($i, j = x, z$) refer to the stress tensor and pre-stress components due to the applied temperature field, respectively. In addition, γ_{ij}^L and ϵ_{ij}^L correspond to the linear terms of the shear and normal strain tensor, respectively, whereas γ_{ij}^{NL} , γ_{ij}^{NL} , and ϵ_{ij}^{NL} are nonlinear terms of the shear and normal strain tensor, respectively. By considering Equations (13) and (33), the variational strain energy, δPE_p , is defined as:

$$\begin{aligned} \delta PE_p = & \int_0^L \left(N_x \frac{d\delta u}{dx} + M_x \left(\frac{5}{4} \frac{d\delta\phi_x}{dx} + \frac{1}{4} \frac{d^2\delta w_0}{dx^2} \right) + \right. \\ & P_x \left(\frac{5}{3h^2} \frac{d\delta\phi_x}{dx} + \frac{5}{3h^2} \frac{d^2\delta w_0}{dx^2} \right) + \\ & \left. N_{xz} \left(\frac{5}{4} \delta\phi_x + \frac{5}{4} \frac{d\delta w_0}{dx} \right) + R_{xz} \left(- \left(\frac{5}{h^2} \delta\phi_x + \frac{5}{h^2} \frac{d\delta w_0}{dx} \right) \right) \right) dx \end{aligned} \tag{35}$$

In addition, the variational energy related to primary stresses (34) δPE_T is defined as:

$$\delta PE_T = \int_0^L N_{0x} \frac{dw_0}{dx} \frac{d\delta w_0}{dx} dx \tag{36}$$

where:

$$\begin{aligned} N_{0x} &= N_{0x}^T + N_{0x}^r \\ N_{0x}^T &= - \int_{-(h_c/2+h_a)}^{h_c/2+h_a} (C_{11}(z)\alpha_x \Delta T) dz \\ N_{0x}^r &= \int_{-(h_c/2+h_a)}^{h_c/2+h_a} V_s \sigma_x^r dz \end{aligned} \tag{37}$$

By substituting Equations (30), (35), and (36) into Equation (28), we obtain the following equations of motion:

$$\begin{aligned} \delta u_0 = 0 \Rightarrow & \partial \frac{\partial N_x}{\partial x} = I_0 \frac{\partial^2 u_0}{\partial t^2} + \frac{1}{4} I_1 \frac{\partial^3 w_0}{\partial x \partial t^2} + \frac{5}{4} I_1 \frac{\partial^2 \phi_x}{\partial t^2} - \frac{10}{6h^2} I_3 \left(\frac{\partial^2 \phi_x}{\partial t^2} + \frac{\partial^3 w_0}{\partial x \partial t^2} \right) \\ \delta \phi_x = 0 \Rightarrow & \frac{5}{4} \frac{\partial M_x}{\partial x} - \frac{5}{3h^2} \frac{\partial P_x}{\partial x} - \frac{5}{4} N_{xz} + \frac{5}{h^2} R_{xz} = \frac{5}{4} I_1 \frac{\partial^2 u_0}{\partial t^2} + \frac{25}{16} I_2 \frac{\partial^2 \phi_x}{\partial t^2} + \\ & \frac{5}{16} I_2 \frac{\partial^3 w_0}{\partial x \partial t^2} - \frac{10}{6h^2} I_3 \frac{\partial^2 u_0}{\partial t^2} - \frac{5}{2h^2} I_4 \frac{\partial^3 w_0}{\partial x \partial t^2} - \frac{25}{6h^2} I_4 \frac{\partial^2 \phi_x}{\partial t^2} + \frac{50}{18h^4} I_6 \frac{\partial^3 w_0}{\partial x \partial t^2} + \\ & \frac{25}{9h^4} I_6 \frac{\partial^2 \phi_x}{\partial t^2} \\ \delta w_0 = 0 \Rightarrow & N_{0x} \frac{\partial^2 w_0}{\partial x^2} - \frac{1}{4} \frac{\partial^2 M_x}{\partial x^2} + \frac{5}{3h^2} \frac{\partial^2 P_x}{\partial x^2} + \frac{5}{4} \frac{\partial N_{xz}}{\partial x} - \frac{5}{h^2} \frac{\partial R_{xz}}{\partial x} = I_0 \frac{\partial^2 w_0}{\partial t^2} \\ & - \frac{1}{4} I_1 \frac{\partial^3 u_0}{\partial x \partial t^2} - \frac{1}{16} I_2 \frac{\partial^4 w_0}{\partial x^2 \partial t^2} - \frac{5}{16} I_2 \frac{\partial^3 \phi_x}{\partial x \partial t^2} + \frac{10}{6h^2} I_3 \frac{\partial^3 u_0}{\partial x \partial t^2} + \frac{5}{2h^2} I_4 \frac{\partial^3 \phi_x}{\partial x \partial t^2} + \\ & \frac{5}{6h^2} I_4 \frac{\partial^4 w_0}{\partial x^2 \partial t^2} - \frac{50}{18h^4} I_6 \frac{\partial^3 \phi_x}{\partial x \partial t^2} - \frac{25}{9h^4} I_6 \frac{\partial^4 w_0}{\partial x^2 \partial t^2} \end{aligned} \tag{38}$$

where the displacement components are assumed as:

$$\begin{aligned} u_0(x, t) &= u_m \cos\left(\frac{m\pi x}{L}\right) e^{i\omega t} \\ \phi_x(x, t) &= \phi_m \cos\left(\frac{m\pi x}{L}\right) e^{i\omega t} \\ w_0(x, t) &= w_m \sin\left(\frac{m\pi x}{L}\right) e^{i\omega t} \end{aligned} \tag{39}$$

and ω refers to the natural frequency.

4. Results and Discussion

The numerical investigation starts with a validation of the proposed model against the literature and continues with a systematic analysis of the thermal buckling and thermal vibration of the sandwich beam for any kinds of thermal distribution, and varying input parameters n , L/h , ε_0 , and V_{SMA} . Thus, our results are first compared to predictions by Kiani and Eslami [39] based on the Euler–Bernoulli theory, as summarized in Table 4 in terms of critical buckling load of the FGM beam with simple supports (S-S) for different values of L/h and volume fraction power, n , under a uniform temperature distribution. As is visible in this table, the good matching between the current formulation and [39] for each value of L/h and volume fraction, n , confirms the accuracy of the proposed formulation, where the Euler–Bernoulli-based approach always yields more conservative results compared to higher-order assumptions, as employed in this work, with the main advantage of treating structural members with higher thicknesses. It is also worth observing that an increased value of L/h and n yields a progressive reduction in the critical buckling load, due to an overall increase in the structural flexibility.

Table 4. Critical buckling load of FGM beam with S-S supports for different value of n and L/h .

L/h	n							
	0		1		2		10	
	Current Study	[39]	Current Study	[39]	Current Study	[39]	Current Study	[39]
0.1	2365.8	2212.88	1030.1	959.01	854.7	797.03	901	851.48
0.05	596.40	545.72	255.09	232.72	211.17	192.66	225.20	206.22
0.025	142.40	128.93	57.03	51.14	46.45	41.56	50.08	44.91
0.013	33.40	29.51	9.53	7.84	6.93	5.52	7.93	6.43

After this validation step, the parametric study starts considering the variation of the critical temperature versus h/L ratio, as shown in Figure 2, as provided by the present formulation and [39], with a reasonable matching among them, with some deviations due to the different theoretical assumptions, especially for higher thicknesses, where a higher order theory seems to be more accurate, accounting for any possible shear effect. Based on the plots in this figure, we note the monotone increase in the critical temperature for an increased h/L ratio, for both a uniform and a linear thermal distribution. A linear distribution, however, always yields higher critical temperatures compared to a uniform distribution under the same geometrical assumptions for the structure.

The numerical investigation continues evaluating comparatively the free vibration of S-S-FGM beams, as estimated by the present model and other formulations from the literature. More specifically, we compare the first dimensionless frequency, $\Omega = \omega L^2/h\sqrt{\rho_m/E_m}$, as provided by our formulation against predictions from a classic beam theory [40] and an FSDT [41], as listed in Table 5, for different values of n and L/h , with a very good agreement among results, all proving the reliability and accuracy of the proposed formulation.

4.1. Thermal Buckling Analysis

In this section, we assess the sensitivity of the buckling response to the length ratio (h/L), volume fraction power (n), initial strain (ε_0), volume fraction (V_{SMA}), and thermal distribution. Figures 3 and 4 show the monotone variation of the critical thermal buckling versus h/L for different values of initial strain and volume fraction of SMA wires within the composite layers, respectively. In both figures, we account for both the TD- and TID-properties of the material, together with a uniform thermal distribution. According to the figures, by increasing ε_0 and V_{SMA} , the critical thermal buckling increases. In addition, the value of the critical thermal buckling for TID-properties is higher than that one for TD properties. Based on the plots in both figures, the critical solutions based on TD and TID material properties assume the same value for low geometrical ratios (i.e., for $h/L = 0.01$), while increasing their differences for higher values of h/L ratios. An increased value of

ϵ_0 and V_{SMA} enables a shift of the curves upwards, with an overall increase in the critical thermal buckling for both TD and TID material properties. In addition, Figure 5 depicts the variation of the critical thermal buckling versus L/h for different values of n , under the double assumption of TD or TID material, together with a uniform thermal distribution and fixed values of $V_{SMA} = 0.2$, $\epsilon_0 = 2\%$, and $h_c/h = 0.8$. As shown in the plots of Figure 5, an enhanced value of n yields an overall increase in the critical thermal buckling, for both TID and TD material properties. Additionally, for a fixed value of n and L/h , the critical thermal buckling associated with TID material properties is always higher than the one related to TD material properties. The main differences among TD- and TID-based results rely on the different phenomenological models, where stress and strain distributions can be clearly affected by temperature together with any possible phase transformation.

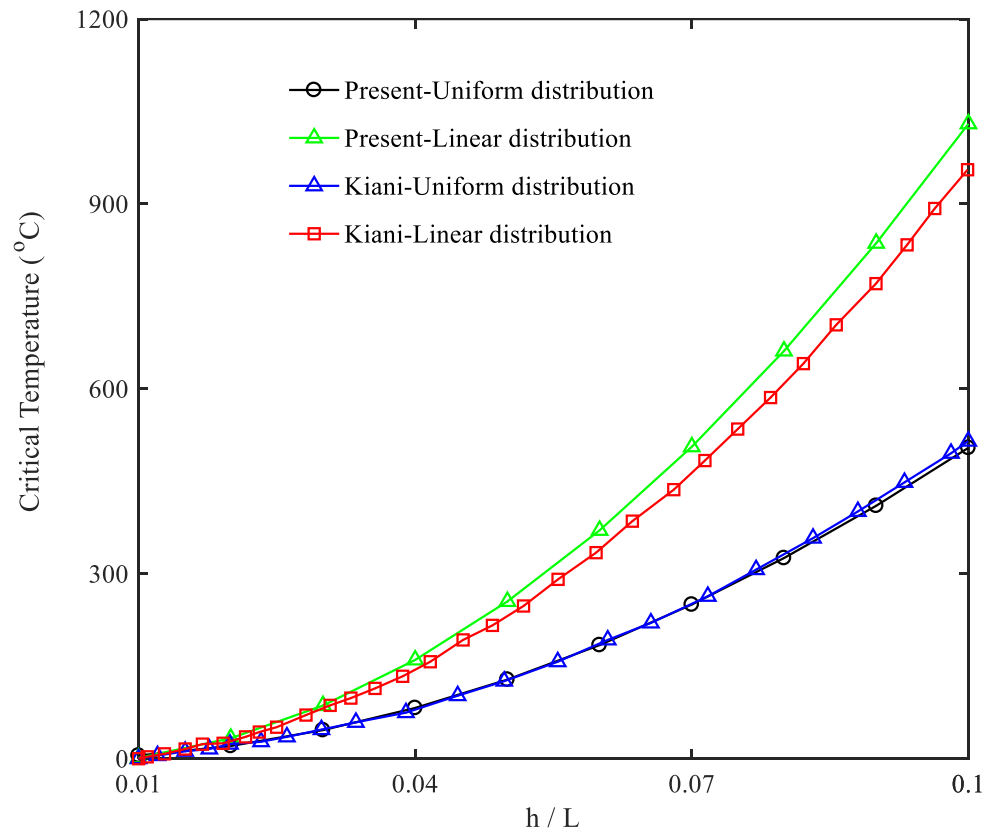


Figure 2. Variation of the critical temperature versus h/L for two types of thermal distribution.

Table 5. First dimensionless frequency for FGM beam with an S-S boundary condition.

L/h	Result	n				
		0	0.1	1	2	10
5	Nejati et al. [41]	6.8470	6.4990	4.8210	4.2510	3.7370
	Aydogdu et al. [40]	6.5632	6.2372	4.6533	4.1025	3.5610
	Present work	6.5134	6.1445	4.6234	4.0671	3.4966
20	Nejati et al. [41]	6.9510	6.5990	4.9070	4.3340	3.8040
	Aydogdu et al. [40]	6.9313	6.5808	4.8950	4.3234	3.7914
	Present work	6.9301	5.5251	4.8942	4.2330	3.7913

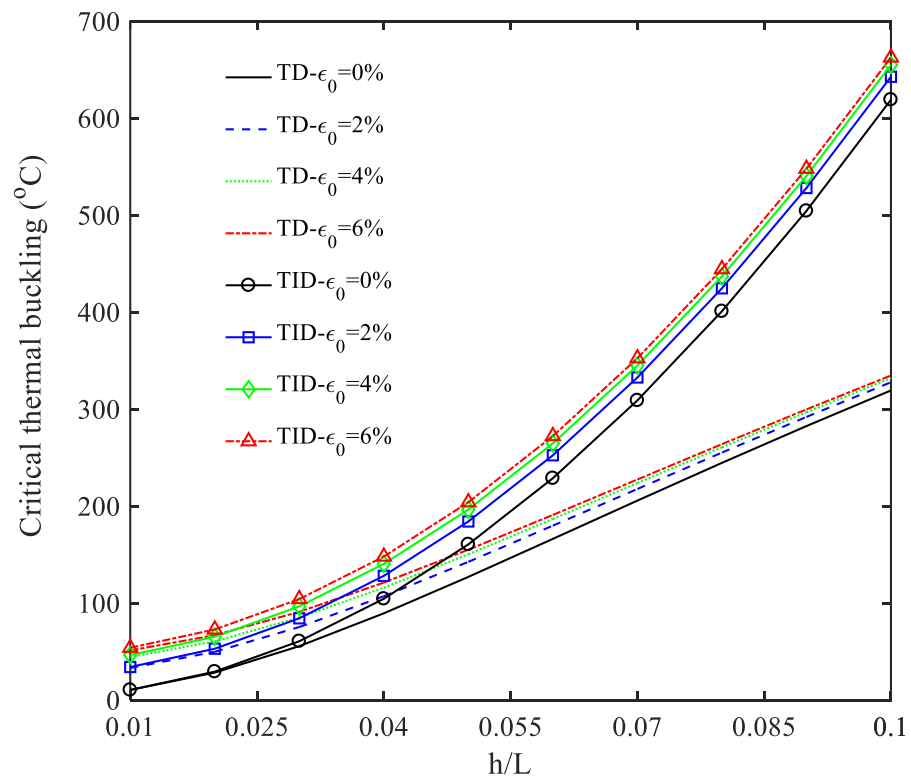


Figure 3. Variation of the critical thermal loading vs. h/L for TD and TID properties, and different values of ϵ_0 ($n = 1, h_c/h = 0.8$ and $V_{SMA} = 0.2$).

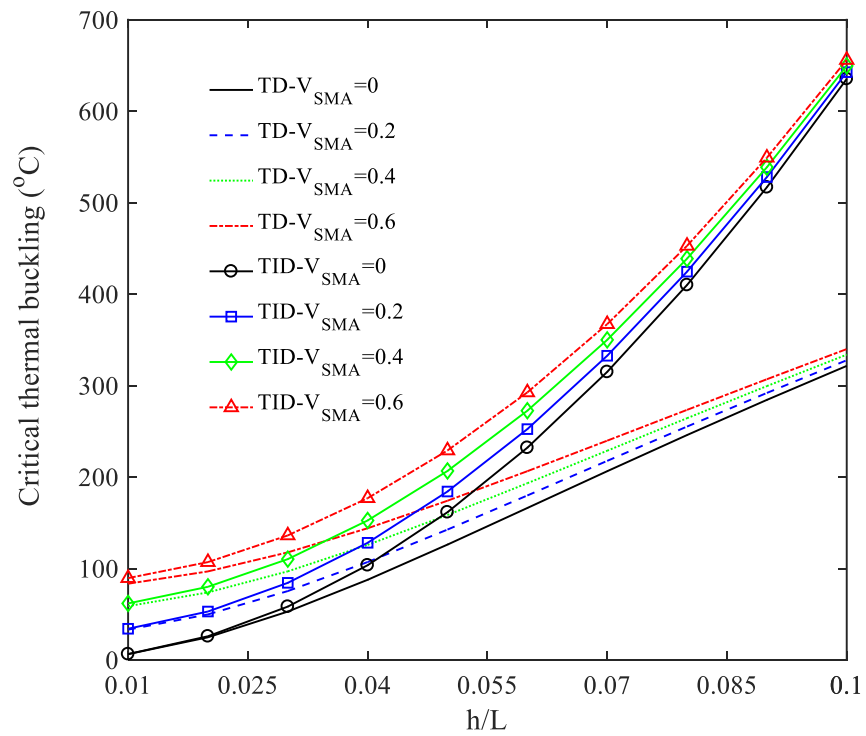


Figure 4. Variation of the critical thermal loading vs. h/L for TD and TID properties and different values of V_{SMA} ($n = 1, h_c/h = 0.8$ and $\epsilon_0 = 2\%$).

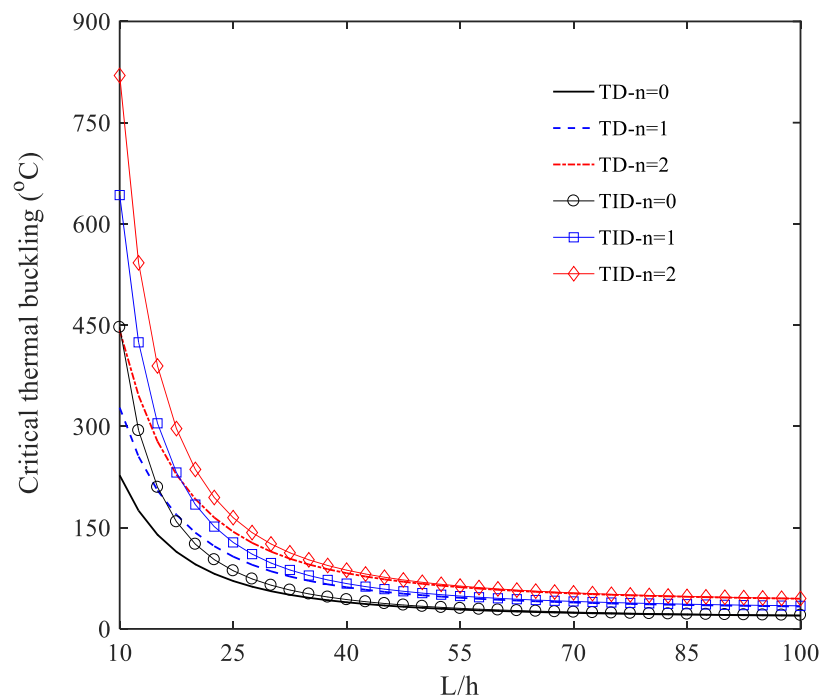


Figure 5. Variation of the critical thermal loading vs. L/h for TD and TID properties, and different values of n ($V_{SMA} = 0.2$, $\varepsilon_0 = 2\%$, $h_c/h = 0.8$).

Such sensitivity of the response to the input value of n seems to reduce gradually, for higher geometrical values of L/h , until the critical thermal buckling becomes totally insensitive to TID or TD material properties.

The influence of linear and uniform thermal distributions on the critical thermal buckling is shown in Figure 6, while varying the geometrical ratio, L/h , from 10 up to 100. As clearly visible from the plots in this figure, the critical thermal buckling obtained for a linear thermal distribution is always higher than the one associated with a uniform distribution, under the same value of V_{SMA} . At the same time, for a fixed thermal distribution, an increased value of V_{SMA} enables increased values of the critical thermal buckling, especially for higher L/h ratios. The effect of ε_0 , V_{SMA} , and n on the critical thermal buckling in linear thermal distribution is shown in Figures 7–9, for L/h ranging from 10 to 100. According to Figures 7 and 8, the initial strain and the volume fraction both provide a similar effect on the critical thermal buckling. Indeed, in both figures the critical thermal buckling increases by increasing ε_0 and V_{SMA} . The effect of ε_0 and V_{SMA} on the critical thermal buckling seems to increase for higher values of L/h . Another parameter affecting the critical thermal buckling response can be the SMA layers thickness (h_a), as depicted in Figure 9 for both linear and uniform thermal distributions, while assuming $n = 1$, $h/L = 0.04$, $V_{SMA} = 0.2$, and $\varepsilon_0 = 2\%$. More specifically, the critical thermal buckling increases by increasing h_a , whereas the critical thermal buckling for a linear distribution is always higher than the one associated with a uniform distribution.

4.2. Thermal Vibration Analysis

In this last section, we focus on the vibration response of the SMA hybrid sandwich beam in a thermal environment. Figures 10–12 depict the variation of the first dimensionless frequency vs. the temperature for a uniform thermal distribution by considering the effect of ε_0 , V_{SMA} , and n , respectively. According to Figures 10 and 11, the first dimensionless frequency tends to decrease for an increased temperature, except for an initial oscillating response for lower temperatures within the starting and ending point of the austenite phase. This effect becomes even more pronounced for higher values of ε_0 and V_{SMA} . A different sensitivity is observed in Figure 12, because the first frequency can increase or

decrease non-monotonically for different settings of the input parameters in terms of n and temperature. In these three figures, the curves intersect at one common point, at which the SMA wires activate. A recovery stress takes place in SMA wires between two distinct points of all the curves due to the enhanced temperature, with a recovery stress induced to the whole structure.

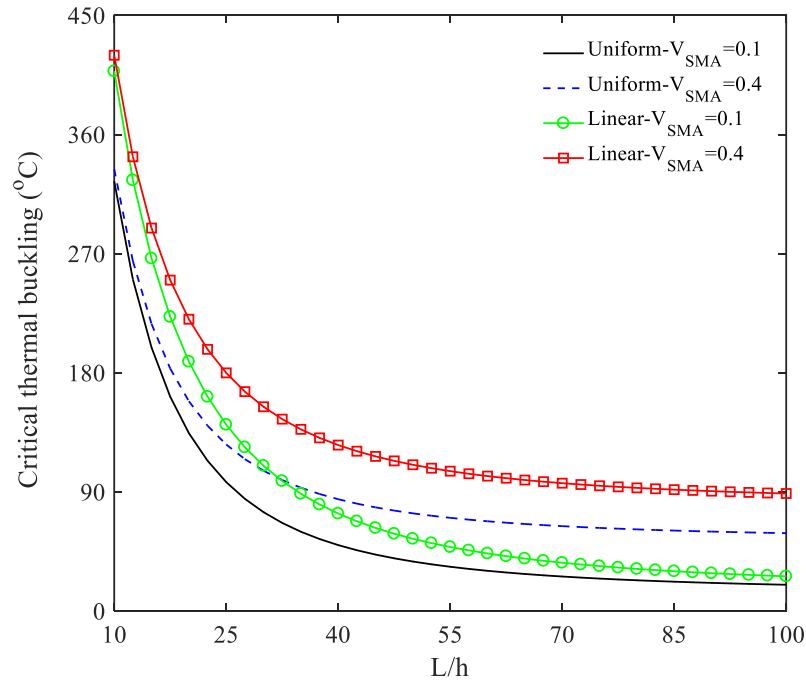


Figure 6. Variation of the critical thermal loading vs. L/h for two types of temperature distribution and different values of V_{SMA} ($n = 1, h_c/h = 0.8$ and $\epsilon_0 = 2\%$).

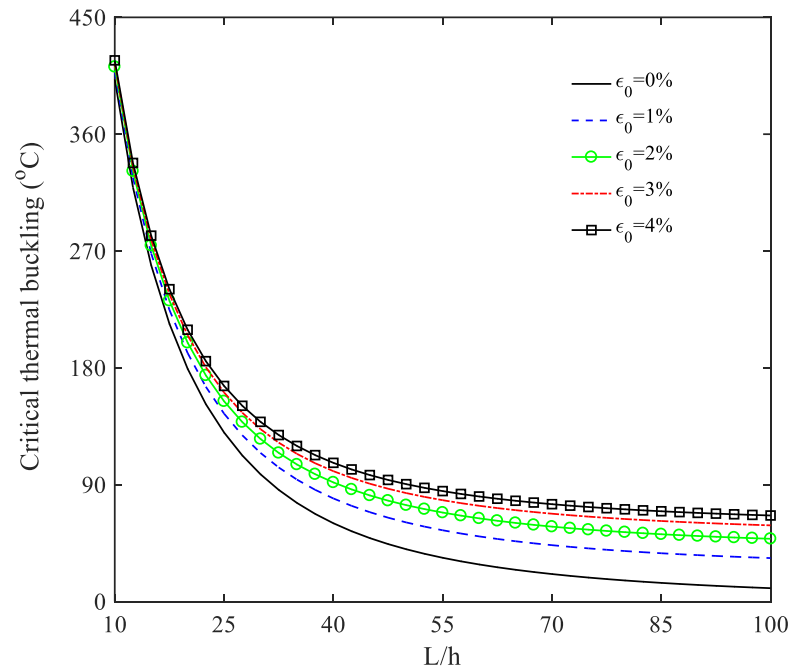


Figure 7. Variation of the critical thermal buckling vs. L/h for a linear distribution and different values of ϵ_0 ($n = 1, h_c/h = 0.8$ and $V_{SMA} = 0.2$).

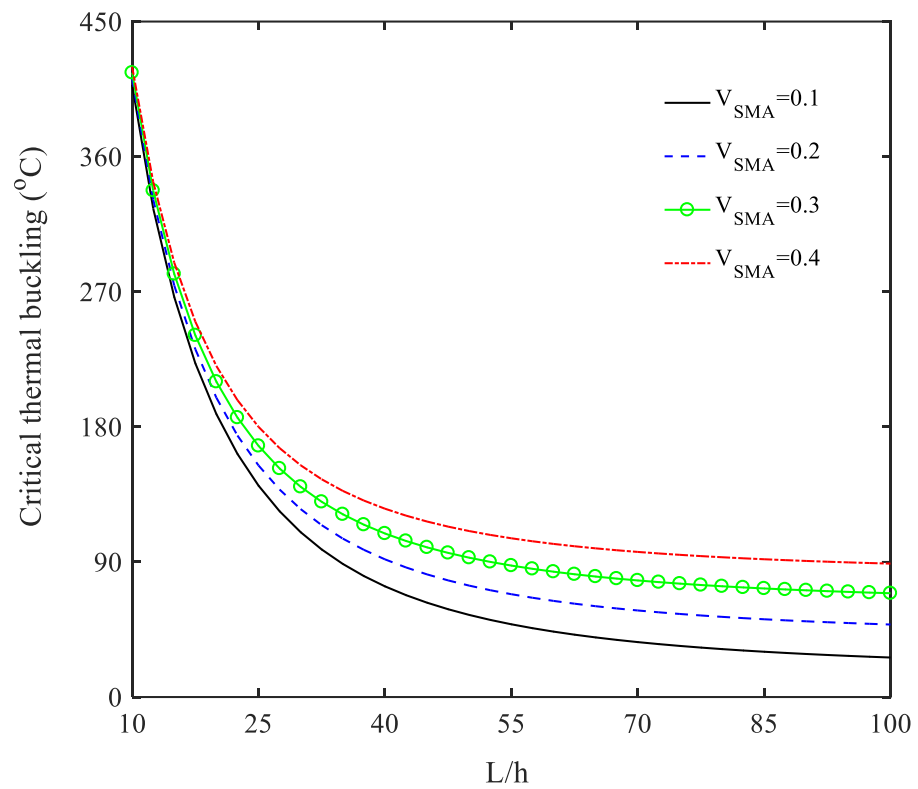


Figure 8. Variation of the critical thermal buckling vs. L/h for a linear distribution and different values of V_{SMA} ($n = 1, h_c/h = 0.8$ and $\epsilon_0 = 2\%$).

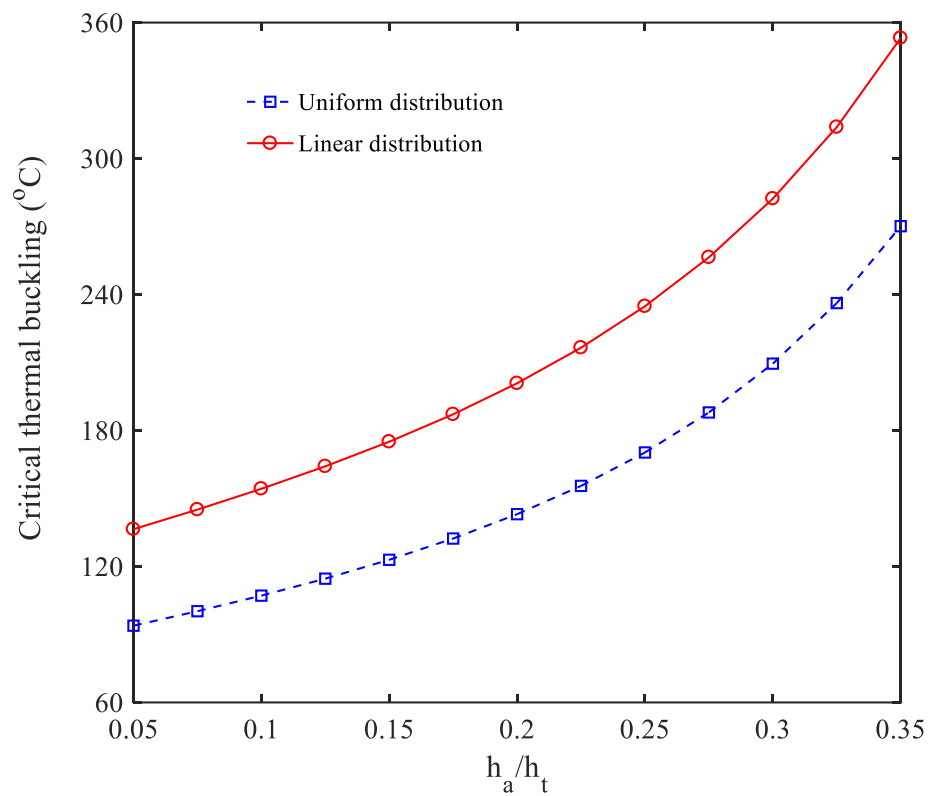


Figure 9. Variation of the critical thermal buckling vs. h_a/h for a linear and uniform thermal distribution ($n = 1, h/L = 0.04, V_{SMA} = 0.2$ and $\epsilon_0 = 2\%$).

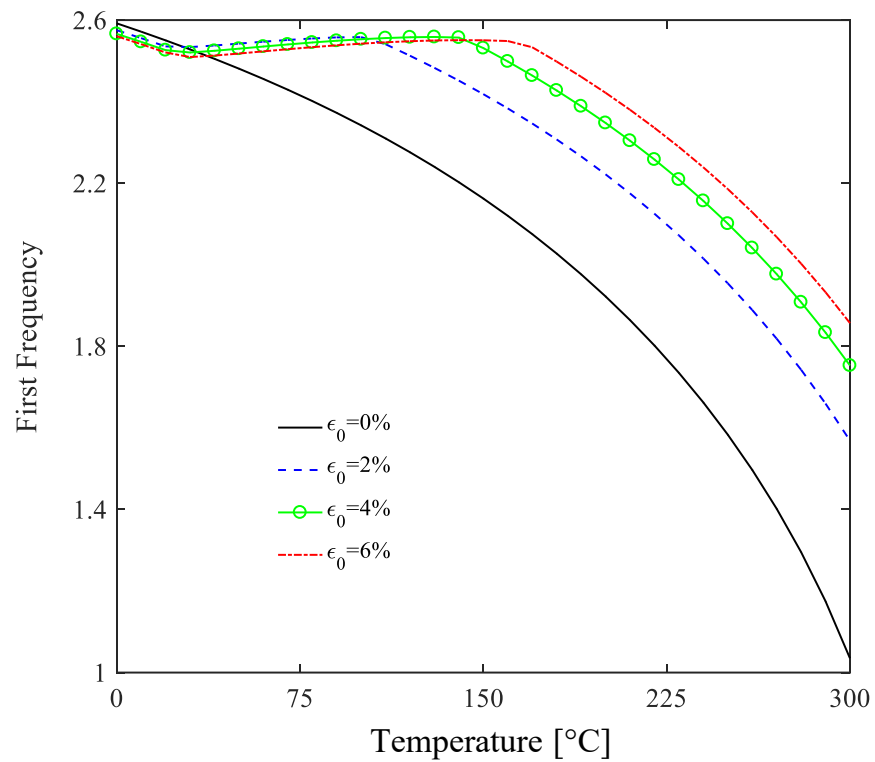


Figure 10. Variation of the first dimensionless frequency vs. temperature for different values of SMA initial pre-strain and a uniform temperature ($V_{SMA} = 0.2, h_c/h = 0.5$ and $n = 1$).

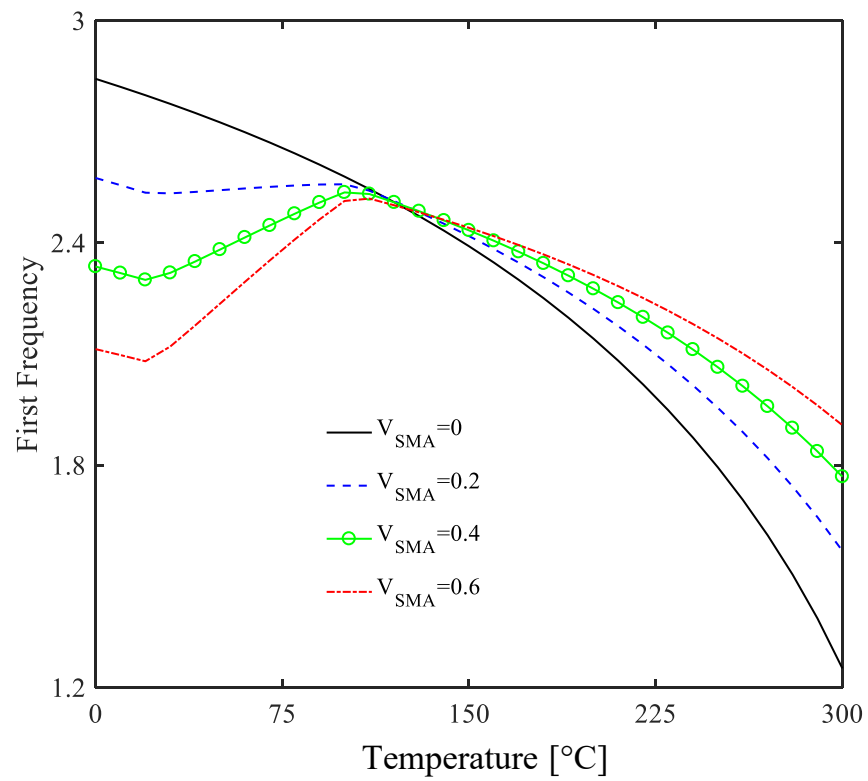


Figure 11. Variation of the first dimensionless frequency vs. temperature for different SMA volume fractions and a uniform temperature ($\epsilon_0 = 2\%, h_c/h = 0.5$ and $n = 1$).

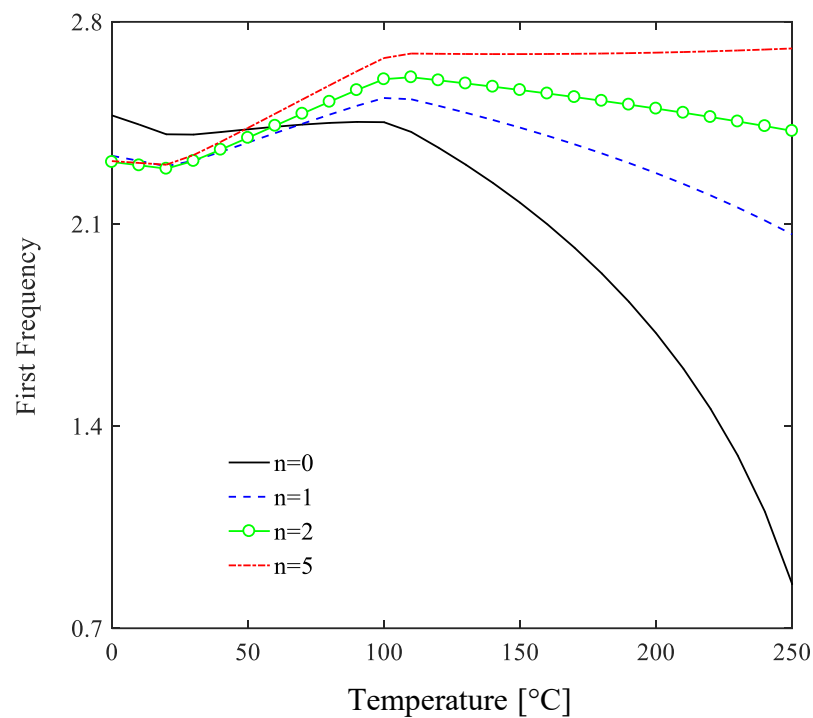


Figure 12. Variation of the first dimensionless frequency vs. temperature for different FGM volume fractions and a uniform temperature ($V_{SMA} = 0.4$, $h_c/h = 0.5$ and $\epsilon_0 = 2\%$).

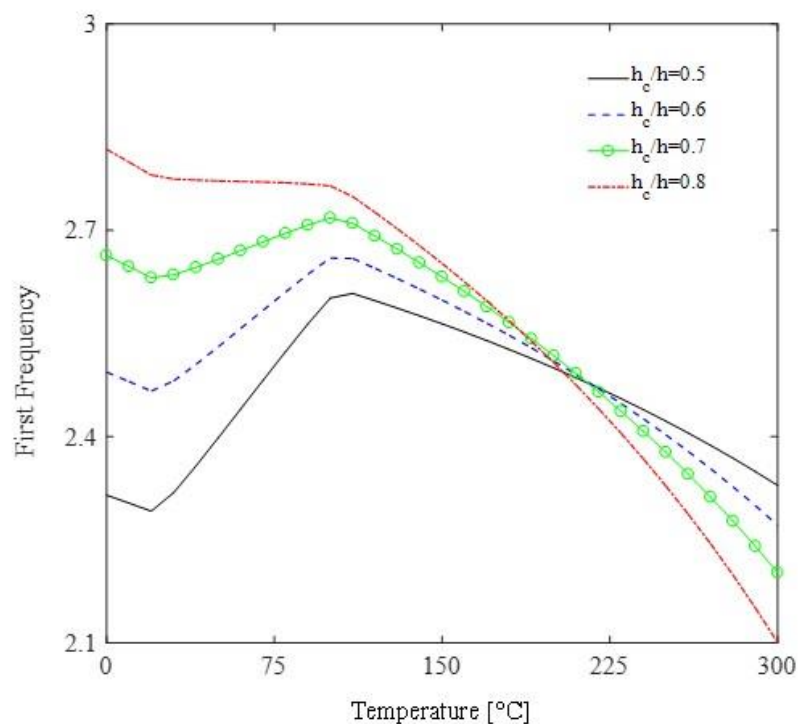


Figure 13. Variation of the first dimensionless frequency vs. temperature for different values of FGM core-to-total thickness ratio and a uniform temperature distribution ($V_{SMA} = 0.4$, $n = 2$ and $\epsilon_0 = 2\%$).

The sensitivity of the vibration response to the core thickness is plotted in Figure 13, under the following assumptions: $V_{SMA} = 0.4$, $n = 2$, $\epsilon_0 = 2\%$, and a uniform thermal distribution. As can be seen in this figure, the core thickness has a very pronounced effect on the first dimensionless frequency. An increased core thickness seems to provide

an increased frequency response for lower temperatures, with a contrary variation of the response for temperatures higher than 200 °C. In Figure 14, we finally plot the variation of the first dimensionless frequency versus temperature by considering TD and TID conditions, under the double assumption of $V_{SMA} = 0.4$ and $V_{SMA} = 0.6$, respectively. According to these plots, the first dimensionless frequency with TID properties is higher than that one for TD properties, whereas an increased value of V_{SMA} yields a reduced value of the first frequency for lower temperatures, and an overall increase for temperatures higher than 100 °C.

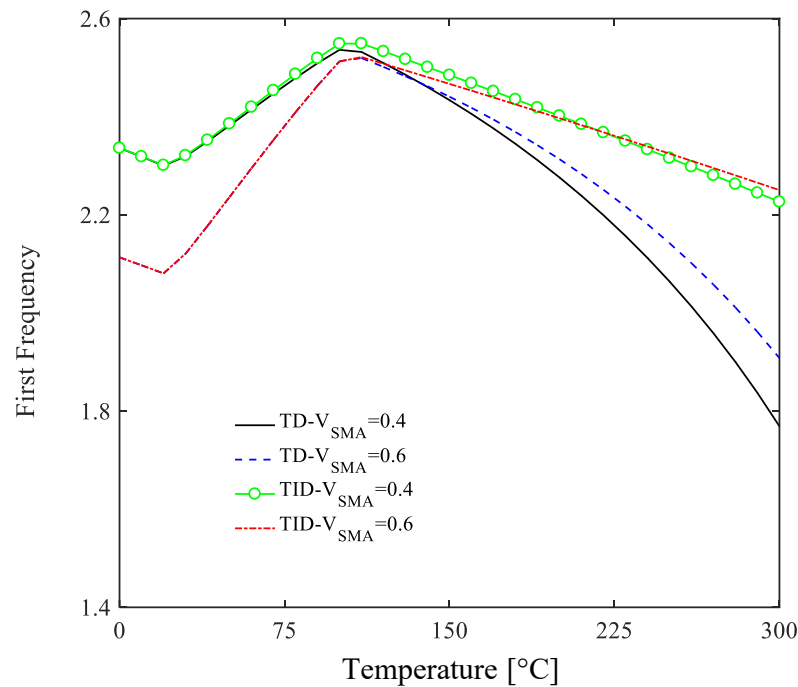


Figure 14. Variation of the first dimensionless frequency vs. temperature for both TD and TID properties, different SMA volume fraction powers, and a uniform temperature distribution ($n = 1$, $h_c/h = 0.5$ and $\varepsilon_0 = 2\%$).

5. Conclusions

The present work has focused on the buckling and free vibration response of a simply supported sandwich beam with an FGM core and external layers reinforced with SMA wires, immersed in a thermal environment. The proposed approach, based on a higher order theory and a variational energy formulation, has been verified in its reliability against predictions from literature, with an accurate response. After this preliminary validation, a systematic study followed for different input parameters, with interesting concluding remarks that could serve as theoretical benchmarks for a further computational treatment of the topic. More specifically, critical thermal buckling has been found to increase for both linear and uniform distributions, by increasing the initial strain field and the reinforcement volume fraction. At the same time, the critical thermal buckling for TD properties is always higher than the one associated with TID properties, especially for higher thicknesses of the structural member. An increased value of n and layer thickness, together with a decreased length-to-thickness ratio, caused an overall enhancement of the critical thermal buckling, which is, in turn, affected by the different thermal distributions assumed in the problem. In detail, the critical thermal buckling, for a linear thermal distribution, always achieves higher values than a uniform distribution. As far as the vibration response is concerned, we have determined the first dimensionless frequency response of the sandwich beam, whose value has been revealed to increase for higher values of ε_0 , V_{SMA} , and n . Moreover, TD and TID properties can affect the first dimensionless frequency, so that the first dimensionless frequency of TID seems to be higher than TD.

Author Contributions: Conceptualization, R.D. and F.T.; Data curation, M.N. and S.S.J.; Formal analysis, M.N., S.S.J., R.D. and F.T.; Investigation, M.N., S.S.J., R.D. and F.T.; Methodology, M.N., S.S.J., R.D. and F.T.; Supervision, R.D. and F.T.; Validation, R.D. and F.T.; Writing—original draft, M.N. and S.S.J.; Writing—review & editing, R.D. and F.T. All authors have read and agreed to the published version of the manuscript.

Funding: This research received no external funding.

Conflicts of Interest: The authors declare no conflict of interest.

Appendix A

The thermomechanical properties of the composite layers reinforced with SAMs are determined as follows:

$$E_{11} = E_s(\xi)V_s + E_c(1 - V_s) \tag{A1}$$

$$G_{12} = G_c \left((1 - \sqrt{V_s}) + \frac{\sqrt{V_s}}{1 - \sqrt{V_s} \left(1 - \frac{G_c}{G_s(\xi)}\right)} \right) \tag{A2}$$

$$G_s(\xi) = \frac{E_s(\xi)}{2(1+\nu_s)} \tag{A3}$$

$$\nu_{12} = \nu_s V_s + \nu_c(1 - V_s) \tag{A3}$$

$$\alpha_{xx} = \frac{V_s \alpha_s E_s(\xi) + (1 - V_s) \alpha_c E_c}{E_{11}} \tag{A4}$$

where the subscripts *c* and *s* refer to the composite matrix and SMAs, respectively. The stress-displacement relations of the problem are detailed in the following:

$$\begin{aligned} N_x &= A_{11} \left(\frac{du_0}{dx} + \frac{1}{2} \left(\frac{dw_0}{dx} \right)^2 \right) + \frac{5}{4} B_{11} \frac{d\phi_x}{dx} - \frac{5}{3h^2} H_{11} \frac{d\phi_x}{dx} + \\ &\frac{1}{4} B_{11} \frac{d^2 w_0}{dx^2} - \frac{5}{3h^2} H_{11} \frac{d^2 w_0}{dx^2} + N_x^T + N_x^r \\ M_x &= B_{11} \left(\frac{du_0}{dx} + \frac{1}{2} \left(\frac{dw_0}{dx} \right)^2 \right) + \frac{5}{4} D_{11} \frac{d\phi_x}{dx} - \frac{5}{3h^2} F_{11} \frac{d\phi_x}{dx} + \\ &\frac{1}{4} D_{11} \frac{d^2 w_0}{dx^2} - \frac{5}{3h^2} F_{11} \frac{d^2 w_0}{dx^2} + M_x^T + M_x^r \\ P_x &= H_{11} \left(\frac{du_0}{dx} + \frac{1}{2} \left(\frac{dw_0}{dx} \right)^2 \right) + \frac{5}{4} F_{11} \frac{d\phi_x}{dx} - \frac{5}{3h^2} G_{11} \frac{d\phi_x}{dx} + \\ &\frac{1}{4} F_{11} \frac{d^2 w_0}{dx^2} - \frac{5}{3h^2} G_{11} \frac{d^2 w_0}{dx^2} + P_x^T + P_x^r \\ N_{xz} &= \frac{5}{4} A_{55} \phi_x - \frac{5}{h^2} D_{55} \phi_x + \frac{5}{4} A_{55} \frac{dw_0}{dx} - \frac{5}{h^2} D_{55} \frac{dw_0}{dx} \\ R_{xz} &= \frac{5}{4} D_{55} \phi_x - \frac{5}{h^2} F_{55} \phi_x + \frac{5}{4} D_{55} \frac{dw_0}{dx} - \frac{5}{h^2} F_{55} \frac{dw_0}{dx} \end{aligned} \tag{A5}$$

To simplify the above equation, the following coefficients are introduced:

$$\begin{aligned} A_{11} &= \int_{-h_c/2}^{h_c/2} C_{11}^{FGM} dz + \int_{h_c/2}^{h_c/2+h_a} C_{11}^{Top\ layer} dz + \int_{-h_c/2}^{-(h_c/2+h_a)} C_{11}^{Bottom\ layer} dz \\ B_{11} &= \int_{-h_c/2}^{h_c/2} Z C_{11}^{FGM} dz + \int_{h_c/2}^{h_c/2+h_a} Z C_{11}^{Top\ layer} dz + \int_{-h_c/2}^{-(h_c/2+h_a)} Z C_{11}^{Bottom\ layer} dz \\ D_{11} &= \int_{-h_c/2}^{h_c/2} Z^2 C_{11}^{FGM} dz + \int_{h_c/2}^{h_c/2+h_a} Z^2 C_{11}^{Top\ layer} dz + \int_{-h_c/2}^{-(h_c/2+h_a)} Z^2 C_{11}^{Bottom\ layer} dz \\ H_{11} &= \int_{-h_c/2}^{h_c/2} Z^3 C_{11}^{FGM} dz + \int_{h_c/2}^{h_c/2+h_a} Z^3 C_{11}^{Top\ layer} dz + \int_{-h_c/2}^{-(h_c/2+h_a)} Z^3 C_{11}^{Bottom\ layer} dz \\ F_{11} &= \int_{-h_c/2}^{h_c/2} Z^4 C_{11}^{FGM} dz + \int_{h_c/2}^{h_c/2+h_a} Z^4 C_{11}^{Top\ layer} dz + \int_{-h_c/2}^{-(h_c/2+h_a)} Z^4 C_{11}^{Bottom\ layer} dz \\ G_{11} &= \int_{-h_c/2}^{h_c/2} Z^6 C_{11}^{FGM} dz + \int_{h_c/2}^{h_c/2+h_a} Z^6 C_{11}^{Top\ layer} dz + \int_{-h_c/2}^{-(h_c/2+h_a)} Z^6 C_{11}^{Bottom\ layer} dz \\ A_{55} &= \int_{-h_c/2}^{h_c/2} C_{55}^{FGM} dz + \int_{h_c/2}^{h_c/2+h_a} C_{55}^{Top\ layer} dz + \int_{-h_c/2}^{-(h_c/2+h_a)} C_{55}^{Bottom\ layer} dz \\ D_{55} &= \int_{-h_c/2}^{h_c/2} Z^2 C_{55}^{FGM} dz + \int_{h_c/2}^{h_c/2+h_a} Z^2 C_{55}^{Top\ layer} dz + \int_{-h_c/2}^{-(h_c/2+h_a)} Z^2 C_{55}^{Bottom\ layer} dz \\ F_{55} &= \int_{-h_c/2}^{h_c/2} Z^4 C_{55}^{FGM} dz + \int_{h_c/2}^{h_c/2+h_a} Z^4 C_{55}^{Top\ layer} dz + \int_{-h_c/2}^{-(h_c/2+h_a)} Z^4 C_{55}^{Bottom\ layer} dz \end{aligned} \tag{A6}$$

and:

$$\begin{aligned}
 N_x^T &= -\int_{-(h_c/2+h_a)}^{h_c/2+h_a} C_{11}(z)\alpha_x\Delta T dz \\
 N_x^r &= \int_{-(h_c/2+h_a)}^{-h_c/2} \sigma_x^r dz + \int_{h_c/2}^{h_c/2+h_a} \sigma_x^r dz \\
 M_x^T &= -\int_{-(h_c/2+h_a)}^{h_c/2+h_a} zC_{11}(z)\alpha_x\Delta T dz \\
 M_x^r &= \int_{-(h_c/2+h_a)}^{-h_c/2} z\sigma_x^r dz + \int_{h_c/2}^{h_c/2+h_a} z\sigma_x^r dz \\
 P_x^T &= -\int_{-(h_c/2+h_a)}^{h_c/2+h_a} z^3C_{11}(z)\alpha_x\Delta T dz \\
 P_x^r &= \int_{-(h_c/2+h_a)}^{-h_c/2} z^3\sigma_x^r dz + \int_{h_c/2}^{h_c/2+h_a} z^3\sigma_x^r dz
 \end{aligned} \tag{A7}$$

Finally, the deviation of force resultants from the initial equilibrium state read as follows:

$$\begin{aligned}
 N_x^1 &= A_{11} \frac{du_0^1}{dx} + \frac{5}{4} B_{11} \frac{d\phi_x^1}{dx} - \frac{5}{3h^2} H_{11} \frac{d\phi_x^1}{dx} + \frac{1}{4} B_{11} \frac{d^2w_0^1}{dx^2} - \frac{5}{3h^2} H_{11} \frac{d^2w_0^1}{dx^2} \\
 M_x^1 &= B_{11} \frac{du_0^1}{dx} + \frac{5}{4} D_{11} \frac{d\phi_x^1}{dx} - \frac{5}{3h^2} F_{11} \frac{d\phi_x^1}{dx} + \frac{1}{4} D_{11} \frac{d^2w_0^1}{dx^2} - \frac{5}{3h^2} F_{11} \frac{d^2w_0^1}{dx^2} \\
 P_x^1 &= H_{11} \frac{du_0^1}{dx} + \frac{5}{4} F_{11} \frac{d\phi_x^1}{dx} - \frac{5}{3h^2} G_{11} \frac{d\phi_x^1}{dx} + \frac{1}{4} F_{11} \frac{d^2w_0^1}{dx^2} - \frac{5}{3h^2} G_{11} \frac{d^2w_0^1}{dx^2} \\
 N_{xz}^1 &= \frac{5}{4} A_{55} \phi_x^1 - \frac{5}{h^2} D_{55} \phi_x^1 + \frac{5}{4} A_{55} \frac{dw_0^1}{dx} - \frac{5}{h^2} D_{55} \frac{dw_0^1}{dx} \\
 R_{xz}^1 &= \frac{5}{4} D_{55} \phi_x^1 - \frac{5}{h^2} F_{55} \phi_x^1 + \frac{5}{4} D_{55} \frac{dw_0^1}{dx} - \frac{5}{h^2} F_{55} \frac{dw_0^1}{dx}
 \end{aligned} \tag{A8}$$

References

- Feli, S.; Jafari, S. Analytical investigation of perforation of aluminum—Foam sandwich panels under ballistic impact. *J. Modares Mech. Eng.* **2013**, *13*, 52–59.
- Arunkumar, M.P.; Jagadeesh, M.; Pitchaimani, J.; Gangadharan, K.V.; LeninBabu, M.C. Sound radiation and transmission loss characteristics of a honeycomb sandwich panel with composite facings: Effect of inherent material damping. *J. Sound Vib.* **2016**, *383*, 221–232. [\[CrossRef\]](#)
- Ameri, B.; Moradi, M.; Talebitooti, R. Effect of Honeycomb Core on Free Vibration Analysis of Fiber Metal Laminate (FML) Beams Compared to Conventional Composites. *Compos. Struct.* **2021**, *261*, 113281. [\[CrossRef\]](#)
- Feli, S.; Jafari, S.S. Analytical modeling for perforation of foam-composite sandwich panels under high-velocity impact. *J. Braz. Soc. Mech. Sci. Eng.* **2017**, *39*, 401–412. [\[CrossRef\]](#)
- Duc, N.D.; Seung-Eock, K.; DucTuan, N.; Tran, P.; DinhKhoa, N. New approach to study nonlinear dynamic response and vibration of sandwich composite cylindrical panels with auxetic honeycomb core layer. *Aerosp. Sci. Technol.* **2017**, *70*, 396–404. [\[CrossRef\]](#)
- Sobhani Aragh, B.; Yas, M.H. Effect of continuously grading fiber orientation face sheets on vibration of sandwich panels with FGM core. *Int. J. Mech. Sci.* **2011**, *53*, 628–638. [\[CrossRef\]](#)
- Lagoudas, D.C. *Shape memory alloys: Modeling and Engineering Applications*; Springer: Berlin/Heidelberg, Germany, 2008.
- Samadpour, M.; Sadighi, M.; Shakeri, M.; Zamani, H.A. Vibration analysis of thermally buckled SMA hybrid composite sandwich plate. *Compos. Struct.* **2015**, *119*, 251–263. [\[CrossRef\]](#)
- Salim, M.; Bodaghi, M.; Kamarian, S.; Shakeri, M. Free vibration analysis and design optimization of SMA/Graphite/Epoxy composite shells in thermal environments. *Lat. Am. J. Solids Struct.* **2018**, *15*. [\[CrossRef\]](#)
- Rasid, Z.A.; Ayob, A.; Zahari, R.; Mustapha, F.; Abang Haji Abdul Majid, D.L.; Varatharajoo, R. Thermal Buckling and Post-Buckling Improvements of Laminated Composite Plates Using Finite Element Method. *Key Eng. Mater.* **2011**, *471–472*, 536–541. [\[CrossRef\]](#)
- Panda, S.K.; Singh, B. Nonlinear finite element analysis of thermal post-buckling vibration of laminated composite shell panel embedded with SMA fibre. *Aerosp. Sci. Technol.* **2013**, *29*, 47–57. [\[CrossRef\]](#)
- Karimiasl, M.; Ebrahimi, F.; Akgöz, B. Buckling and post-buckling responses of smart doubly curved composite shallow shells embedded in SMA fiber under hygro-thermal loading. *Compos. Struct.* **2019**, *223*, 110988. [\[CrossRef\]](#)
- Yuan, G.; Bai, Y.; Jia, Z.; Lau, K.; Hung, P. Structural deformation performance of glass fiber reinforced polymer composite beam actuated by embedded indented SMA wires. *Compos. Part B* **2019**, *159*, 284–291. [\[CrossRef\]](#)
- Girish, J.; Ramachandra, L. Thermal postbuckled vibrations of symmetrically laminated composite plates with initial geometric imperfections. *J. Sound Vib.* **2005**, *282*, 1137–1153. [\[CrossRef\]](#)
- Kamarian, S.; Shakeri, M. Thermal buckling analysis and stacking sequence optimization of rectangular and skew shape memory alloy hybrid composite plates. *Compos. Part B* **2017**, *116*, 137–152. [\[CrossRef\]](#)

16. Roh, J.H.; Oh, I.K.; Yang, S.M.; Han, J.H.; Lee, I. Thermal post-buckling analysis of shape memory alloy hybrid composite shell panels. *Smart Mater. Struct.* **2004**, *13*, 1337–1344. [[CrossRef](#)]
17. Mansouri, M.H.; Shariyat, M. Thermal buckling predictions of three types of high-order theories for the heterogeneous orthotropic plates, using the new version of DQM. *Compos. Struct.* **2014**, *113*, 40–55. [[CrossRef](#)]
18. Li, Z.M. Thermal postbuckling behavior of 3D braided beams with initial geometric imperfection under different type temperature distributions. *Compos. Struct.* **2014**, *108*, 924–936. [[CrossRef](#)]
19. Asadi, H.; Kiani, Y.; Shakeru, M.; Eslami, M.R. Exact solution for nonlinear thermal stability of hybrid laminated composite Timoshenko beams reinforced with SMA fibers. *Compos. Struct.* **2014**, *108*, 811–822. [[CrossRef](#)]
20. Khdeir, A.A. Thermal buckling of cross-ply laminated composite beams. *Acta Mech.* **2001**, *149*, 201–213. [[CrossRef](#)]
21. Bayat, Y.; EkhteraeiToussi, H. Exact solution of thermal buckling and post buckling of composite and SMA hybrid composite beam by layerwise theory. *Aerosp. Sci. Technol.* **2017**, *67*, 484–494. [[CrossRef](#)]
22. Yongsheng, R.; Chenggang, D.; Yuyan, S. Nonlinear Free and Forced Vibration Behavior of Shear-Deformable Composite Beams with Shape Memory Alloy Fibers. *Shock Vib.* **2016**, *2016*, 1056087. [[CrossRef](#)]
23. Chen, Q.; Levy, C. Vibration analysis and control of flexible beam by using smart damping structures. *Compos. Part B* **1999**, *30*, 395–406. [[CrossRef](#)]
24. Park, J.S.; Kim, J.H.; Moon, S.H. Vibration of thermally post-buckled composite plates embedded with shape memory alloy fibers. *Compos. Struct.* **2004**, *63*, 179–188. [[CrossRef](#)]
25. Parhi, A.; Singh, B.N. Nonlinear free vibration analysis of shape memory alloy embedded laminated composite shell panel. *Mech. Adv. Mater. Struct.* **2017**, *24*, 713–724. [[CrossRef](#)]
26. Nekouei, M.; Raghebi, M.; Mohammadi, M. Free vibration analysis of hybrid laminated composite cylindrical shells reinforced with shape memory alloy fibers. *J. Vib. Control* **2019**, *26*, 610–626. [[CrossRef](#)]
27. Rogers, C.; Barker, D. Experimental studies of active strain energy tuning of adaptive composites. In Proceedings of the 31st Structures, Structural Dynamics and Materials Conference, Long Beach, CA, USA, 2–4 April 1990.
28. Asadi, H.; Bodaghi, M.; Shakeri, M.; Aghdam, M.M. On the free vibration of thermally pre/post-buckled shear deformable SMA hybrid composite beams. *Aerosp. Sci. Technol.* **2013**, *31*, 73–86. [[CrossRef](#)]
29. Alambeigi, K.; Mohammadimehr, M.; Bamdad, M.; Rabczuk, T. Free and forced vibration analysis of a sandwich beam considering porous core and SMA hybrid composite face layers on Vlasov's foundation. *Acta Mech.* **2020**, *231*, 3199–3218. [[CrossRef](#)]
30. Brinson, L.C. One dimensional constitutive behavior of shape memory alloys: Thermomechanical derivation with non-constant material functions and redefined martensite internal variable. *J. Intell. Mater. Syst. Struct.* **1993**, *4*, 229–242. [[CrossRef](#)]
31. Asadi, H.; Kiani, Y.; Shakeri, M.; Eslami, M.R. Exact Solution for Nonlinear Thermal Stability of Geometrically Imperfect Hybrid Laminated Composite Timoshenko Beams Embedded with SMA Fibers. *J. Eng. Mech.* **2015**, *141*, 04014144. [[CrossRef](#)]
32. Reddy, J.N.; Chin, C.D. Thermomechanical Analysis of Functionally Graded Cylinders and Plates. *J. Therm. Stresses* **1998**, *21*, 593–626. [[CrossRef](#)]
33. Shen, H.S. *Functionally Graded Materials: Nonlinear Analysis of Plates and Shells*; CRC Press: Boca Raton, FL, USA, 2016.
34. Reddy, J.N. *Mechanics of Laminated Composite Plates and Shells: Theory and Analysis*; CRC Press: Boca Raton, FL, USA, 2003.
35. Reddy, J.N. *Energy Principles and Variational Methods in Applied Mechanics*; John Wiley & Sons: Hoboken, NJ, USA, 2017.
36. Brush, D.O.; Almroth, B.O.; Hutchinson, J.W. Buckling of Bars, Plates, and Shells. *J. Appl. Mech.* **1975**, *42*, 911. [[CrossRef](#)]
37. Nejati, M.; Yas, M.H.; Eslampanah, A.H.; Bagheriasl, M. Extended three-dimensional generalized differential quadrature method: The basic equations and thermal vibration analysis of functionally graded fiber orientation rectangular plates. *Mech. Adv. Mater. Struct.* **2017**, *24*, 854–870. [[CrossRef](#)]
38. Nejati, M.; Fard, K.M.; Eslampanah, A.; Jafari, S.S. Free vibration analysis of reinforced composite functionally graded plates with steady state thermal conditions. *Lat. Am. J. Solids Struct.* **2017**, *14*, 886–905. [[CrossRef](#)]
39. Kiani, Y.; Eslami, M.R. Thermal buckling analysis of functionally graded material beams. *Int. J. Mech. Mater. Des.* **2010**, *6*, 229–238. [[CrossRef](#)]
40. Aydogdu, M.; Taskin, V. Free vibration analysis of functionally graded beams with simply supported edges. *Mater. Des.* **2007**, *28*, 1651–1656. [[CrossRef](#)]
41. Nejati, M.; Fard, K.M.; Eslampanah, A. Effects of fiber orientation and temperature on natural frequencies of a functionally graded beam reinforced with fiber. *J. Mech. Sci. Technol.* **2015**, *29*, 3363–3371. [[CrossRef](#)]